Cellular/Molecular

The Plasma Membrane-Associated GTPase Rin Interacts with the Dopamine Transporter and Is Required for Protein Kinase C-Regulated Dopamine Transporter Trafficking

Deanna M. Navaroli,[2]* Zachary H. Stevens,[1]* Zeljko Uzelac,[5] Luke Gabriel,[3] Michael J. King,[1] Lawrence M. Lifshitz,[4] Harald H. Sitte,[5] and Haley E. Melikian[1]

[1]Brudnick Neuropsychiatric Research Institute, Department of Psychiatry, [2]Interdisciplinary Graduate Program, Graduate School of Biomedical Sciences, [3]Graduate Program in Neuroscience, and [4]Program in Molecular Medicine, University of Massachusetts Medical School, Worcester, Massachusetts 01655, and [5]Medical University Vienna, Center for Physiology and Pharmacology, Institute of Pharmacology, 1090 Vienna, Austria

Dopaminergic signaling and plasticity are essential to numerous CNS functions and pathologies, including movement, cognition, and addiction. The amphetamine- and cocaine-sensitive dopamine (DA) transporter (DAT) tightly controls extracellular DA concentrations and half-life. DAT function and surface expression are not static but are dynamically modulated by membrane trafficking. We recently demonstrated that the DAT C terminus encodes a PKC-sensitive internalization signal that also suppresses basal DAT endocytosis. However, the cellular machinery governing regulated DAT trafficking is not well defined. In work presented here, we identified the Ras-like GTPase, Rin (for Ras-like in neurons) (Rit2), as a protein that interacts with the DAT C-terminal endocytic signal. Yeast two-hybrid, GST pull down and FRET studies establish that DAT and Rin directly interact, and colocalization studies reveal that DAT/Rin associations occur primarily in lipid raft microdomains. Coimmunoprecipitations demonstrate that PKC activation regulates Rin association with DAT. Perturbation of Rin function with GTPase mutants and shRNA-mediated Rin knockdown reveals that Rin is critical for PKC-mediated DAT internalization and functional downregulation. These results establish that Rin is a DAT-interacting protein that is required for PKC-regulated DAT trafficking. Moreover, this work suggests that Rin participates in regulated endocytosis.

Introduction

Presynaptic neurotransmitter reuptake facilitated by plasma membrane transporters is the primary mechanism terminating synaptic transmission. Dopamine transporter (DAT) terminates DA signaling and thus is central to controlling extracellular DA levels in the brain (Torres and Amara, 2007). DAT is the primary target for therapeutic agents such as methylphenidate (Ritalin) and bupropion (Wellbutrin), as well as the addictive psychostimulants amphetamine and cocaine, whose actions inhibit DAT function (Iversen, 2006). Recent knock-in transgenic mouse studies demonstrated that DAT availability is paramount to establishing the rewarding properties of cocaine (Chen et al., 2006), and aberrant DAT function was reported recently in a subgroup of attention-deficit hyperactivity disorder (ADHD) patients (Mazei-Robison et al., 2008). Moreover, $DAT^{+/-}$ and $DAT^{-/-}$ mice are hyperlocomotive and exhibit significant DA depletion in tissue stores (Gainetdinov et al., 1998; Jones et al., 1998). Thus, mechanisms that regulate DAT plasma membrane availability are likely to have a significant impact on DA signaling and the availability of DAT to interact with therapeutic and addictive drugs.

A wealth of data demonstrates that DAT activity is acutely downregulated by protein kinase C (PKC) activation, resulting in DAT trafficking to, and sequestering in, endosomal vesicles (Torres et al., 2003; Melikian, 2004). Work from our laboratory established that DAT C-terminal residues 587–596 encode endocytic regulatory domain that modulates both basal and PKC-enhanced DAT internalization rates (Holton et al., 2005; Boudanova et al., 2008). The DAT N terminus is also central to regulating DAT endocytic trafficking (Sorkina et al., 2009), and Nedd4–2-mediated ubiquitination in this domain is critical for PKC-mediated DAT sequestration (Sorkina et al., 2006; Miranda et al., 2007). A variety of proteins have been identified that interact with DAT, including PICK1 (Torres et al., 2001; Bjerggaard et al., 2004), Hic-5 (Carneiro et al., 2002), synaptogyrin-3 (Egaña et al., 2009), and calcium/calmodulin-dependent kinase II (CaMKII) (Fog et al., 2006). However, none of these identified DAT-interacting proteins are mechanistically linked to PKC-regulated DAT internalization. In the current study, we sought to identify proteins that (1) interacted with DAT endocytic regulatory residues 587–596 and (2) were required for PKC-regulated DAT trafficking. A yeast two-hybrid screen identified the Rin (for

Received May 27, 2011; revised July 18, 2011; accepted Aug. 1, 2011.

Author contributions: D.M.N., Z.U., H.H.S., and H.E.M. designed research; D.M.N., Z.H.S., Z.U., L.G., M.J.K., and H.E.M. performed research; D.M.N., Z.H.S., L.M.L., H.H.S., and H.E.M. analyzed data; H.H.S. and H.E.M. wrote the paper.

*D.M.N. and Z.H.S. contributed equally to this work.

This work was supported by NIH Grant DA15169 (H.E.M.) and Austrian Science Fund/FWF, Sonderforschungsbereich 3506 (H.H.S.). We thank Drs. Mary Munson, Doug Andres, and David Lambright for insightful discussions and Dr. Stephen Baker for excellent biostatistics support.

Correspondence should be addressed to Dr. Haley E. Melikian, Brudnick Neuropsychiatric Research Institute, Department of Psychiatry, University of Massachusetts Medical School, 303 Belmont Street, Worcester, MA 01604. E-mail: haley.melikian@umassmed.edu.

DOI:10.1523/JNEUROSCI.2649-11.2011

Copyright © 2011 the authors 0270-6474/11/3113758-13$15.00/0

Ras-like in neurons) GTPase as a candidate DAT-interacting protein. Using biochemical, cellular imaging, and knockdown approaches, we determined that Rin interacts directly with DAT in a PKC-regulated manner and is required for PKC-mediated DAT internalization.

Materials and Methods

Materials. Monoclonal rat anti-DAT antibodies were from Millipore Bioscience Research Reagents and mouse anti-Rin antibodies (clone 27G2) were from ExAlpha Biologics or Millipore. Rabbit anti-DAT polyclonal antibody was a generous gift from Dr. Roxanne Vaughan (University of North Dakota, Grand Forks, ND). cDNAs encoding HA–RinQ78L and HA–RinS34N (Spencer et al., 2002a) were kindly provided by Dr. Doug Andres (University of Kentucky, Lexington, KY). Mouse anti-green fluorescent protein (GFP) antibody and rat anti-HA antibody (clone 3F10) were from Roche, and mouse anti-actin antibody was from Santa Cruz Biotechnology. Mouse anti-HA (HA.11) antibody was acquired from Covance. Horseradish peroxidase (HRP)-conjugated secondary antibodies were from either Millipore Bioscience Research Reagents (anti-mouse) or Santa Cruz Biotechnology (anti-rat), and goat anti-mouse Fc fragment coupled to horseradish peroxidase was from Jackson ImmunoResearch. Fluorescently conjugated secondary antibodies and transferrin were from Invitrogen. [^{3}H]DA (dihydroxyphenylethylamine 3,4-[ring-2,5,6,-^{3}H]) was from PerkinElmer Life and Analytical Sciences, and sulfo-NHS-SS-biotin was from Pierce. Phorbol 12-myristate 13-acetate (PMA) and GBR12909 (1-[2-[bis(4-fluorophenyl)-methoxy]ethyl]-4-[3-phenylpropyl] piperazine) were from Tocris Cookson. All other chemicals and reagents were from Sigma-Aldrich and Thermo Fisher Scientific and were of the highest grade available.

Yeast two-hybrid screen. A bait encoding human DAT amino acids 587–596 was constructed by amplifying hDAT cDNA region 1778–1807 with primers containing NotI and BglII sites and was cloned in-frame into the pSOS vector (Stratagene) at the NotI/BglII sites. The pSOS–DAT(586–597) bait was used to screen a CytoTrap XR substantia nigra cDNA library cloned into the pMyr vector (Stratagene). Positive interactions rescue Ras activity and permit yeast growth at the restrictive temperature. Positive clones were picked and underwent secondary and tertiary screening to rule out false positives attributable to temperature reversion. Plasmid DNA was isolated from tertiary positive clones, transformed into DH5αE bacteria (Invitrogen), amplified in liquid culture, and purified, and sequences were determined (Genewiz).

Cell culture and transfections. PC12 cells were maintained at 37°C, 10% CO_2 in DMEM (high glucose), 5% horse serum (Hyclone), and 5% bovine calf serum (Invitrogen) supplemented with 2 mM glutamine, 10^2 U/ml penicillin/streptomycin. Stably transfected PC12 cells expressing wild-type and 587–590(4A) DAT were maintained as described previously (Melikian and Buckley, 1999; Loder and Melikian, 2003; Boudanova et al., 2008) under selective pressure with 0.2 mg/ml G418 (Invitrogen). HEK293 cells were grown in DMEM, 10% fetal bovine serum, 2 mM glutamine, and 10^2 U/ml penicillin/streptomycin, 37°C, 5% CO_2. The human neuroblastoma cell line SK-N-MC was obtained from American Type Culture Collection and was maintained in MEM supplemented with 10% fetal bovine serum, 2 mM glutamine, and 10^2 U/ml penicillin/streptomycin, 37°C, 5% CO_2. HEK293 cells were transiently transfected with Lipofectamine 2000, according to the instructions of the manufacturer, using 2 μg of total DNA/7 $\times$ 10^5 cells, incubating with DNA/Lipofectamine complexes with cells 4 h for maximal cell viability. PC12 cells were transfected either by electroporation or using Lipofectamine 2000. For electroporation, 18.2 μg of DNA/1.1 $\times$ 10^7 PC12 cells in 0.75 ml of electroporation buffer (in mM: 137 NaCl, 5.0 KCl, 0.7 Na_2HPO_4, 6.0 glucose, and 20 HEPES, pH 7.05) was combined in 4 mm cuvettes and were electroporated using an exponential decay protocol at 300 V, 500 μF. Cells were resuspended in PC12 media supplemented with 3 mM EGTA and recovered 30 min, 37°C with occasional inversion. Cells were collected by centrifugation, resuspended in PC12 media, and plated as indicated. For Lipofectamine 2000 transfections, PC12 cells were seeded 1 d before transfection at 1 $\times$ 10^6 cells per well (six-well plates coated with 0.5 mg/ml poly-D-lysine; biochemical assays) or 2.25 $\times$ 10^5 per well (glass coverslips coated with 1.0 mg/ml poly-D-lysine for microscopy) in antibiotic-free PC12 media. Cells were transfected with either 4 μg (six-well plates) or 0.8 μg (glass coverslips) total DNA at a 2.5:1 Lipofectamine/DNA ratio, according to the instructions of the manufacturer. Transfection solutions were replaced with fresh antibiotic-free media 16–24 h after transfection, and cells were assayed as described for each experiment. For SK-N-MC cells, 2.25 $\times$ 10^5 cells per well were plated 1 d before transfection in antibiotic-free media on either glass coverslips coated with 0.25 mg/ml poly-D-lysine (microscopy) or in uncoated 24-well tissue cultureware plates (uptake assays). Cells were transfected with 0.3 μg of total DNA per well at a 2:1 Lipofectamine/DNA ratio, according to the instructions of the manufacturer. Transfection solutions were replaced with fresh, antibiotic-free media 4 h after transfection, and cells were assayed as described for each experiment.

Coimmunoprecipitations. One $\times$ 10^6 PC12 or PC12 cells stably expressing either wild-type or 587–590(4A) DAT were seeded in poly-D-lysine-coated six-well plates 1 d before experiments. Cells were treated as indicated, lysed in coimmunoprecipitation (co-IP) buffer (50 mM Tris, pH 7.4, 100 mM NaCl, 1% Triton X-100, 10% glycerol, and 1 mM EDTA) containing protease inhibitors (1.0 mM PMSF and 1.0 μg/ml each leupeptin, aprotinin, and pepstatin) and phosphatase inhibitors (10 mM sodium fluoride and 1 mM sodium orthovanadate), 30 min, 4°C with gentle shaking. Lysates were cleared by centrifugation (4°C), and protein concentrations were determined using the BCA Protein Assay (Pierce) with BSA standards. Equivalent amounts of cellular protein underwent immunoprecipitation (overnight, 4°C) using Protein A/G beads (Pierce) precoated with the indicated antibodies. Supernatants were concentrated with Millipore spin filtration columns (10 kDa molecular weight cutoff), and beads were washed three times with co-IP buffer. Proteins were eluted by boiling in SDS-PAGE sample buffer containing 2 M urea (final concentration), and proteins were separated on 10% SDS-PAGE gels. After transfer to nitrocellulose, immunoblots were blocked with 5% nonfat dry milk, 0.1% Tween 20, and PBS, and proteins were detected with the indicated primary antibodies. To avoid detecting mouse IgG light chain in the immunoprecipitation complex, immunoreactive Rin bands were detected with goat anti-mouse F_c fragment coupled to HRP. Standard secondary antibodies conjugated to HRP were used to detect all other immunoreactive proteins. HRP-positive bands were visualized by reacting with Dura West Substrate (Pierce) and imaging with a VersaDoc imaging system (Bio-Rad). Nonsaturating bands were quantified using Quantity One software (Bio-Rad) and were normalized to the amount of DAT immunoprecipitated in the same reaction.

glutathione S-transferase pull downs. hDAT cDNA nucleotides 1778–1879, corresponding to DAT amino acids 587–617, were amplified by PCR, and the product was cloned into the pGEX-5x-1 vector (GE Healthcare) downstream of and in-frame with glutathione *S*-transferase (GST). The DAT 587–590(4A) mutation was generated using QuikChange Mutagenesis (Stratagene), and all construct sequences were confirmed by dideoxy chain termination sequencing (Genewiz). Plasmids were transformed into *Escherichia coli* BL21 and were cultured and induced with isopropyl-β-D-thiogalactopyranoside at 28°C to minimize fusion protein degradation, although some degradation was apparent in many of the assays. Fusion proteins were purified with glutathione agarose according to the instructions of the manufacturer, and protein purification was monitored at each step by SDS-PAGE with Coomassie staining. For pull downs, PC12 postnuclear supernatants were prepared with a ball-bearing cell homogenizer as described previously (Melikian and Buckley, 1999). The indicated amount of cell homogenate was incubated with equivalent amounts of glutathione agarose bound to GST, GST–DAT 587–617, or GST–DAT 587–590(4A), 37°C, 1 h. Beads were washed three times with 50 mM Tris, pH 7.4, 150 mM NaCl, 1 mM EDTA, 1% Triton X-100, and 10% glycerol and were boiled in SDS-PAGE sample buffer, 5 min to elute bound proteins. Samples were resolved on SDS-PAGE gels and were immunoblotted for Rin and GST (to confirm pull down). Nonsaturating Rin bands were imaged as described above for coimmunoprecipitations, normalizing to GST band densities (GST + GST–DAT in cases when degradation occurred).

Fluorescence resonance energy transfer (FRET) (Schmid and Sitte, 2003) was measured with a Carl Zeiss Axiovert 200 epifluorescence mi-

croscope. The "three-filter method" was performed as described previously (Bartholomaus et al., 2008). Images were taken using 63× oil-immersion objectives and Ludl filter wheels allowing a rapid excitation and emission filter exchange. We used HEK293 cells that were maintained and transiently transfected with plasmid cDNA (1.7 μg) by means of the calcium phosphate coprecipitation method as described previously (Sucic et al., 2010). The Ludl filter wheels were configured as follows: cyan fluorescent protein (CFP) (I_{Donor}; excitation, 436 nm; emission, 480 nm; and dichroic mirror, 455 nm), yellow fluorescent protein (YFP) ($I_{Acceptor}$; excitation, 500 nm; emission, 535 nm; and dichroic mirror, 515 nm), and FRET (I_{FRET}; excitation, 436 nm; emission, 535 nm; and dichroic mirror, 455 nm). Images were taken with a CCD camera (Coolsnap *fx*; Roper Scientific). Background fluorescence was subtracted from all images. We analyzed the images pixel by pixel using NIH ImageJ (version 1.43b; Wayne Rasband, National Institutes of Health, Bethesda, MD) and the NIH ImageJ plug-in PixFRET (pixel-by-pixel analysis of FRET with NIH ImageJ, version 1.5.0; Feige et al., 2005) with which spectral bleed-through parameters for the donor bleed through (BT) and the acceptor BT were determined and normalized FRET image (N_{FRET}) was calculated in the following way:

$$N_{FRET} = \frac{I_{FRET} - BT_{Donor} * I_{Donor} - BT_{Acceptor} * I_{Acceptor}}{\sqrt{I_{Donor} * I_{Acceptor}}} * 100,$$

The mean N_{FRET} was measured at the plasma membrane (predefined as the region of interest) using the computed N_{FRET} image. The regions of interest were selected in the CFP (donor) or YFP (acceptor) image (to avoid bleaching-associated bias) and transmitted to the N_{FRET} image by the NIH ImageJ Multi Measure Tool. As negative control, we used the CFP-labeled form of DAT or Rin with a membrane-bound form of YFP (Hein et al., 2005) that was kindly provided by Viacheslav Nikolaev (University of Würzburg, Würzburg, Germany). As positive controls for membrane proteins, we used the serotonin transporter (SERT) tagged with CFP and YFP on its cytoplasmic N and C termini, respectively (to yield C-SERT-Y; Just et al., 2004). We tagged DAT and Rin with CFP and YFP to reveal C-DAT and Y-DAT (Bartholomaus et al., 2008) as well as C-Rin and Y-Rin to compare the FRET values in Rin and DAT (and rule out any bias introduced by the different tags, although they differ only in a few amino acids). We also transfected HEK293 cells with combinations of C-DAT and Y-DAT as well as C-Rin and Y-Rin. The statistical significance of differences between the experimental conditions was determined using one-way ANOVA followed by Tukey's multiple comparison test.

Immunocytochemistry and microscopy. Cells were transfected with the indicated cDNAs at a 1:1 ratio and were assayed 48 h after transfection. Cells were treated as indicated, rinsed in PBS, and fixed in 4% paraformaldehyde prepared in PBS, 10 min, 25°C. Cells were blocked and permeabilized in blocking solution (PBS, 1% IgG/protease-free BSA, 5% goat serum, and 0.2% Triton X-100), 30 min, room temperature, followed by incubation with the indicated primary antibodies, 45 min, 25°C. Cells were washed with PBS and incubated with Alexa Fluor 594-, Alexa Fluor 405-, and Alexa Fluor 488-conjugated secondary antibodies (as indicated), 45 min, 25°C. Cells were washed with PBS, dried, and mounted on glass slides with ProLong Gold mounting medium (Invitrogen). Immunoreactive cells were visualized as described previously (Holton et al., 2005) with a Carl Zeiss Axiovert 200M microscope using a 63×, 1.4 numerical aperture oil-immersion objective, and 0.4 μm optical sections were captured through the *z*-axis with a Retiga-1300R cooled CCD camera (Qimaging) using Slidebook 5.0 software (Intelligent Imaging Innovations). *z*-stacks were deconvolved with a constrained iterative algorithm using measured point-spread functions for each fluorescent channel. All images shown are single 0.4 μm planes through the center of each cell. For CTX colocalization studies, before fixing and staining cells, cells were incubated with 2.0 μg/ml Alexa Fluor 594-conjugated cholera toxin subunit B (CTX), 1 h, 4°C and were washed extensively in PBS^{2+} and 0.2% IgG/protease-free BSA. To quantify the percentage of DAT that colocalized with Rin (by volume, i.e., counting voxels) in CTX-positive and CTX-negative regions, we assessed each *z*-stack over a broad range of threshold triplets (i.e., a threshold for each of the three channels). Given the inherent signal intensity variability among cells and to avoid biasing our analysis, a range of thresholds (picked manually while viewing three-dimensional images) was deliberately set to be somewhat wider than the likely range. The lowest threshold allowed for some diffuse background fluorescence to remain; the highest threshold clearly was eroding the margins of labeled structures. Colocalization percentages were calculated at 10 equally spaced thresholds for each species, resulting in 1000 colocalization pairs for each cell. For each cell, we examined the sensitivity (to the threshold) of the raft and nonraft colocalization percentages by creating a surface plot for the two percentages. A Wilcoxon's matched-pairs signed-rank test indicated significant difference across all thresholds. Therefore, single measurements at the median threshold were chosen for statistical analysis and data presentation.

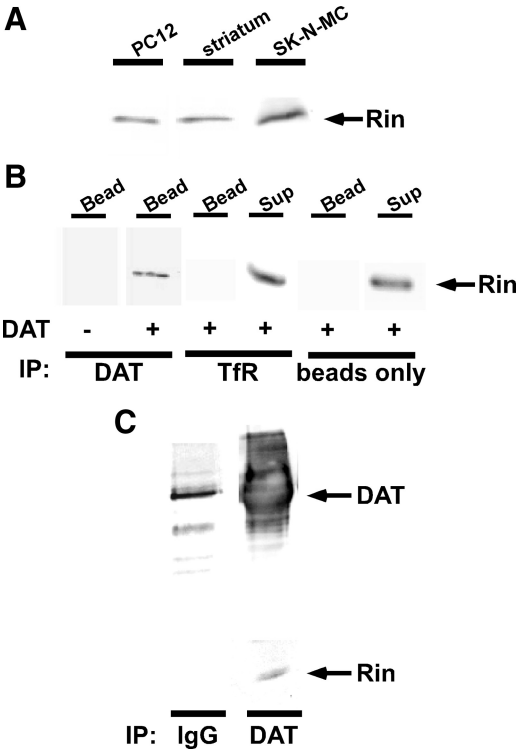


Figure 1. Rin is expressed in PC12 cells and rat striatum and specifically coimmunoprecipitates with DAT. ***A***, Rin expression in catecholaminergic tissue and cell lines. Twenty micrograms of PC12 and SK-N-MC lysate and 150 μg of rat striatal lysate were resolved by SDS-PAGE and immunoblotted with mouse anti-Rin antibodies. ***B***, Coimmunoprecipitations. DAT was immunoprecipitated from equivalent amounts lysate from PC12 cells transfected with either vector (−) or DAT (+). Control immunoprecipitations were performed using anti-TfR antibodies or with Protein A/G beads alone. Bead eluents (Bead) and $^1/_{10}$th supernatant volumes (Sup) were resolved by SDS-PAGE and immunoblotted with an anti-Rin antibody. Representative blots are shown ($n = 3$). ***C***, Coimmunoprecipitations from rat striatal synaptosomes. Immunoprecipitations were performed with solubilized rat striatal synaptosomes using Protein A beads coated with rabbit anti-DAT antibodies or rabbit IgG alone. Eluents were resolved by SDS-PAGE, and immunoreactive bands were detected with the indicated antibodies. A representative blot is shown ($n = 2$).

Internalization assay. Relative initial internalization rates were measured using reversible biotinylation as described previously (Loder and Melikian, 2003; Holton et al., 2005; Boudanova et al., 2008). Cells were cotransfected with DAT and the indicated constructs at a 1:2 DAT/other cDNA ratio and were assayed 48–72 h after transfection. Briefly, transfected cells were biotinylated twice, 15 min, 4°C with 2.5 mg/ml NHS-SS-biotin and were quenched twice, 15 min, 4°C with 100 mM glycine. Cells were rapidly warmed to 37°C and incubated with or without 1 μM PMA, 10 min, 37°C, followed by rapidly cooling to 4°C to stop internalization. Residual surface biotin on internalization samples and stripping controls was stripped by reducing twice for 15 min, 4°C with 50

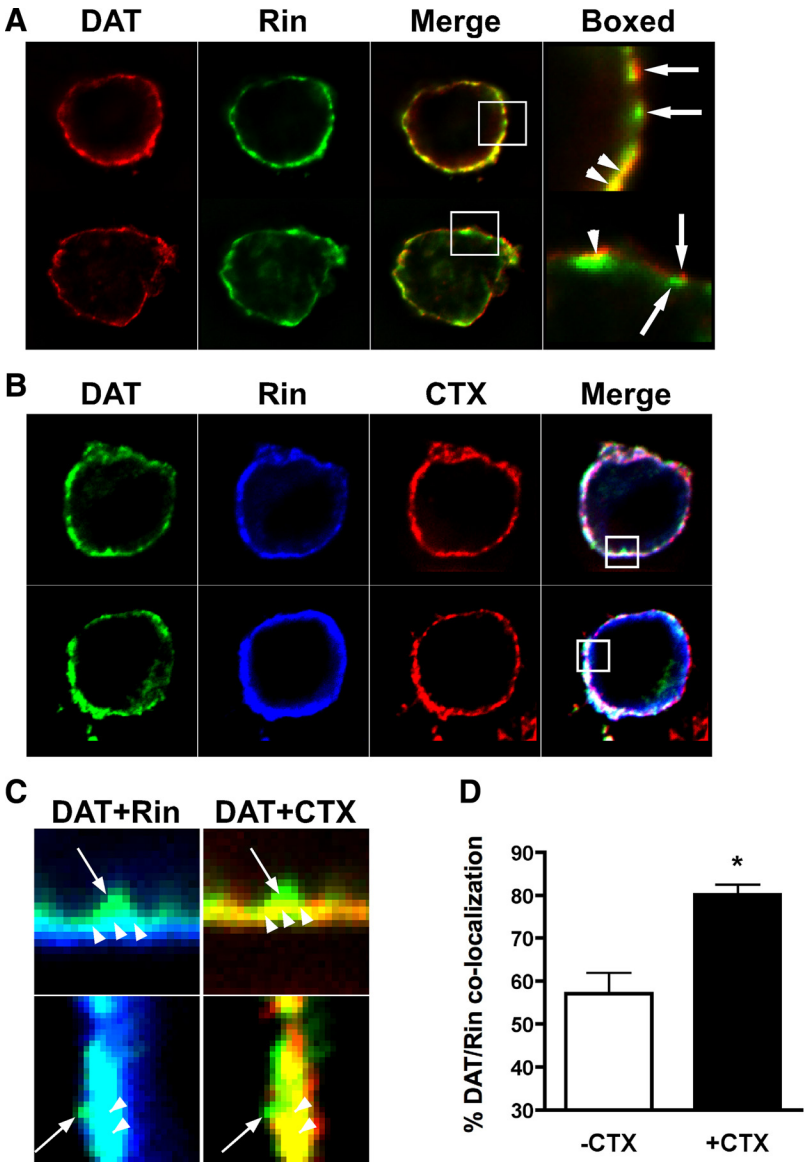


Figure 2. DAT and Rin colocalization at the plasma membrane is enriched in lipid raft microdomains. Immunofluorescence. PC12 cells were cotransfected with DAT and CFP–Rin and were fixed and stained as follows. ***A***, Cells were stained with anti-DAT and anti-GFP antibodies and imaged as described in Materials and Methods. Boxes indicate an enlargement of the areas indicated with white boxes in the merged images. ***B***, Cells were labeled with Alexa Fluor 594 –CTX and were subsequently stained with anti-DAT and anti-GFP antibodies and imaged as described in Materials and Methods. ***C***, Enlargement of the boxed areas from images in ***B***. Arrows indicate DAT-immunoreactive pixels that colocalize with neither Rin (blue) nor CTX (red). Arrowheads indicate foci of DAT/Rin colocalization that also colocalize with CTX. ***D***, Average data. DAT/Rin colocalization in CTX-positive (+CTX) and CTX-negative (−CTX) cell regions was measured at 10 independent thresholds per channel, as described in Materials and Methods. Average data at the median threshold are expressed as percentage ± SEM DAT/Rin colocalization. *$p < 0.0001$, significantly different from −CTX, paired *t* test; $n = 16$.

mM tris(2-carboxyethyl)phosphine. Cells were lysed, and biotinylated proteins were isolated with streptavidin agarose and analyzed by SDS-PAGE and immunoblotting for DAT. Immunoblots were probed in parallel for GFP and HA to confirm cotransfection with CFP–Rin (wild-type) and HA-tagged Rin mutants. Internalization rates were calculated as the percentage DAT internalized over 10 min compared with total surface protein labeled at time 0. Assays were only included if stripping efficiencies were >90%.

Short hairpin studies. Short hairpin RNAs (shRNAs) targeting 29 nt spans of the human Rin mRNA cloned into the pGFP-V-RS vector, which coexpresses turbo GFP, were purchased from Origene. hRin shRNA sequences were as follows: hRin228, GGTCCAGAGAGTACAAGG TGGTAATGCTG.

hRin knockdown efficiencies were assessed in HEK293T cells, taking advantage of their relatively high transfection efficiency. Two × 10^5 cells were seeded into six-well culture plates 1 d before transfection. Cells were transfected using Lipofectamine 2000 (Invitrogen), using 4.0 μg of plasmid DNA per well and a Lipofectamine/DNA ratio of 2.5:1. Media was changed 4 h after transfection, and at 72 h after transfection, GFP-positive cells were enriched by flow cytometry (University of Massachusetts Medical School Flow Cytometry Core Facility). Cells were collected by centrifugation and lysed in RIPA buffer, and Rin levels were measured by quantitative immunoblotting equivalent amounts of cell lysate, normalizing to actin as a loading control. For knockdown experiments, SK-N-MC cells were transfected with Lipofectamine 2000 as described above, with equal amounts of DAT and the indicated plasmids, and were plated on either poly-D-lysine-coated glass coverslips (immunofluorescence) or 24-well tissue cultureware plates (uptake assays). All studies were conducted 72 h after transfection, and shRNA expression was confirmed by detecting GFP coexpression, by microscopy or immunoblot.

Antibody internalization assays. SK-N-MC cells were cotransfected with hDAT encoding an HA epitope tag in the second extracellular loop (ELA–HA–DAT) (Sorkina et al., 2006) and the indicated control or shRNA cDNAs at a 1:1 ratio. At 72 h after transfection, surface DAT was labeled with 2 μg/ml mouse anti-HA antibody, 30 min, room temperature. To monitor PKC-induced internalization, cells were extensively washed and rapidly warmed to 37°C in PBS^{2+} supplemented with 0.2% IgG and protease-free BSA, 0.18% glucose, and 1 μM PMA and were incubated in the same solution, 15 min, 37°C. Cells were rapidly washed in cold PBS to inhibit additional endocytic trafficking and were fixed in 4% paraformaldehyde in PBS, 10 min, room temperature. Residual surface HA antibody was blocked by incubating in 20 μg/ml goat anti-mouse secondary antibody in 5% normal goat serum and 1% IgG/protease-free BSA, 45 min, room temperature. Cells were washed three times in PBS and were permeabilized in 0.2% saponin in PBS containing 1% IgG and protease-free BSA, and 5% normal goat serum, 30 min, room temperature. Internalized HA antibody was detected by probing cells with goat anti-mouse secondary antibody conjugated to Alexa Fluor 594 (1:5000), 45 min, room temperature. Cells were washed three times in PBS, and coverslips were mounted in ProLong Gold. Images of GFP-positive cells were captured as described above for microscopy, using identical exposure times for all cells. For quantification, GFP-positive cells were scored blindly for PMA-induced DAT internalization, which was defined as the presence of multiple large (≥100 nm) intracellular puncta distinct from the plasma membrane and visible in all three cell perspectives (*x–y*, *x–z*, and *y–z* axes). The percentage GFP-positive cells exhibiting PMA-induced DAT internalization for each transfection condition was averaged across multiple experiments, and significant differences in PMA-induced internalization were determined by one-way ANOVA with Dunnett's *post hoc* analysis compared with vector-transfected cells.

[^{3}H]DA uptake assays. Transfected cells were seeded onto 24-well plates, and [^{3}H]DA uptake was measured 48 h after transfection as re-

ported previously (Loder and Melikian, 2003; Boudanova et al., 2008). Briefly, cells were rinsed and preincubated in KRH buffer (120 mM NaCl, 4.7 mM KCl, 2.2 mM $CaCl_2$, 1.2 mM $MgSO_4$, 1.2 mM KH_2PO_4, 0.18% glucose, and 10 mM HEPES, pH 7.4) at for 37°C for 30 min with the indicated drugs. Uptake was initiated by adding 1.0 μM [^{3}H]DA (PerkinElmer Lief and Analytical Sciences) containing 10^{-5} M pargyline and 10^{-5} M ascorbic acid. Assays proceeded for 10 min (37°C) and were terminated by rapidly washing cells with ice-cold KRH buffer. Cells were solubilized in scintillation fluid, and accumulated radioactivity was determined by liquid scintillation counting in a Wallac Microbeta scintillation plate counter. Nonspecific uptake was defined in the presence of 10 μM GBR12909 and averaged <5% of total counts measured. Data analysis was performed using Microsoft Excel and GraphPad Prism Software.

Results

Rin is a DAT-interacting protein

We previously identified a 10 aa region encoded in hDAT C-terminal residues 587–596 that is required for PKC-regulated DAT internalization (Holton et al., 2005) and that negatively regulates basal DAT endocytic rates (Boudanova et al., 2008). Our major aim in the current study was to identify proteins that interacted with the hDAT residues 587–596 (FREKALAYAIA) and that were mechanistically integral to PKC-regulated DAT trafficking. Using this sequence as bait, we used the hSOS rescue system to screen a human substantia nigra cDNA library. The advantage of this approach is that library cDNAs are myristylated and thereby anchored at the plasma membrane, whereas baits are cloned in-frame with the Ras guanine nucleotide exchange factor, hSOS. Thus, interactions between bait and library prey occur at or near the plasma membrane, mimicking circumstances during DAT endocytic trafficking. Screens take place in the temperature-sensitive mutant yeast strain cdc25H, which lacks Ras signaling and is unable to grow at the restrictive temperature. Protein–protein interactions localize hSOS to the plasma membrane, activate Ras signaling, and rescue the temperature-sensitive phenotype. In our initial studies, we attempted to use the entire DAT C terminus as bait. However, this bait alone was capable of rescuing growth in the absence of library coexpression and was thus deemed unsuitable as bait in the library screen. However, the FREKLAYAIA sequence (hDAT residues 587–596) alone did not rescue yeast growth (data not shown) and was therefore used as bait in the screen. We isolated four clones that rescued yeast growth at the restrictive temperature. Sequence analysis revealed that clone H19 corresponded to the small neuronal GTPase Rin, also known as Rit2. Retransforming purified hRin plasmid with the DAT 587–596 bait also yielded a positive interaction and confirmed the protein–protein interaction (data not shown).

We first investigated whether Rin was expressed in dopaminergic cells, to determine whether there was a physiologically relevant context for cellular DAT/Rin interactions. Immunoblots revealed a single 25 kDa immunoreactive band in catecholaminergic cells lines and neuronal tissues, including the rat pheochromocytoma PC12, the human neuroblastoma SK-N-MC, as well as in rat striatum (Fig. 1*A*). In addition to its neuronal expression, we also detected Rin in rat muscle and liver, primary cultured rat astrocytes, and mouse embryonic kidney cells, as well as in non-neuronal cell lines HeLa, COS-1, CHO, IMCD3, and HEK293 (data not shown). Given that the mRNA expression of Rin is reported to be restricted to neuronal tissue (Lee et al., 1996), we were concerned that the anti-Rin antibody might be also detecting Rit, the closest homolog of Rin. Because both proteins are 25 kDa and could not be distinguished on the basis of electrophoretic mobility, we used Rin and Rit GFP fusion proteins to test for this possibility. Both constructs were expressed in PC12 cells and exhibited the expected molecular weight shift, as confirmed by immunoblotting with anti-GFP antibodies (data

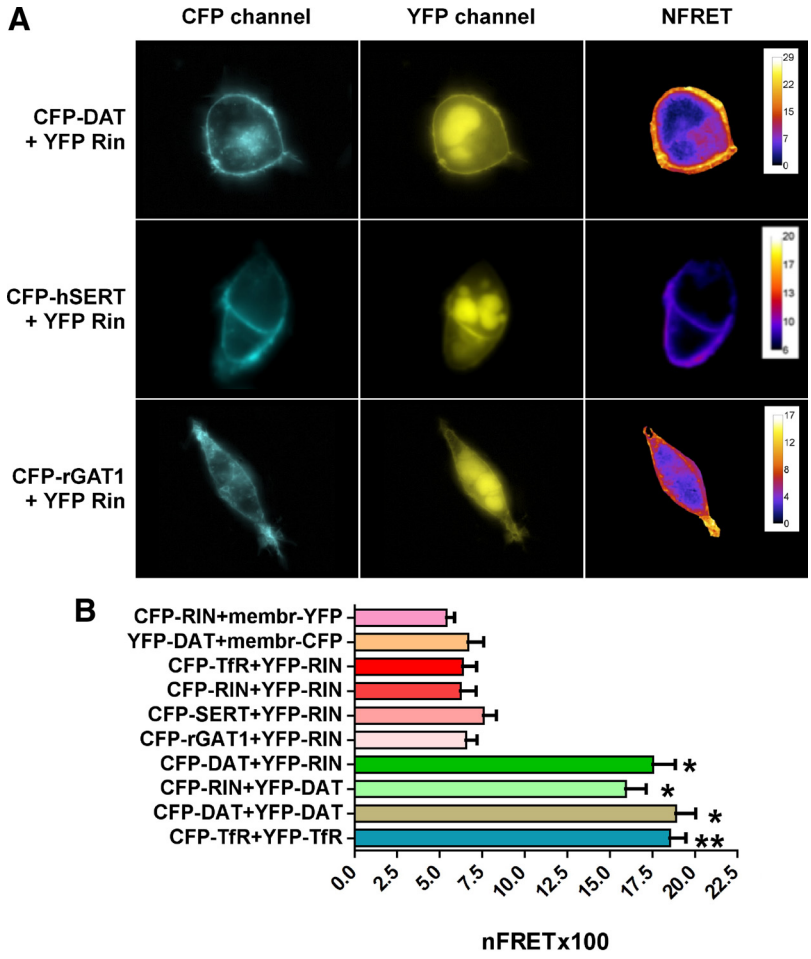


Figure 3. Rin and DAT oligomerization as demonstrated by FRET microscopy in intact cells. HEK293 cells were transiently transfected with cDNAs encoding CFP- or YFP-tagged proteins as indicated, and epifluorescence microscopy was performed 2 d after transfection. ***A***, The first and second columns show images obtained with CFP and YFP filter sets, respectively; the third column displays a corrected and normalized FRET image (N_{FRET}) established with PIXFRET. A look-up table of the color code used is presented in the last column. All images shown are representative of three to seven experiments. In all images, background fluorescence was subtracted. ***B***, Averaged data. Normalized FRET efficiencies (N_{FRET} values) are given for cells expressing the following constructs: C-Rin and membrane-bound YFP (membr-YFP; $n = 15$), Y-DAT and membr-CFP ($n = 25$), C-TfR and Y-Rin ($n = 20$), C-Rin and Y-Rin ($n = 16$), C-SERT and Y-Rin ($n = 27$), C-rGAT1 and Y-Rin ($n = 30$), C-DAT and Y-Rin ($n = 24$), C-Rin and Y-DAT ($n = 20$), C-DAT and Y-DAT ($n = 23$), and C-TfR and Y-TfR ($n = 37$). All values were analyzed by one-way ANOVA with Dunn's multiple comparison test. *$p < 0.001$, significantly different from (YFP–DAT and membr-CFP), (CFP–Rin and YFP–Rin), and (Rin and membr-YFP). **$p < 0.001$, significantly different from (CFP–TfR and YFP–Rin), (CFP–Rin and YFP–Rin), and (Rin and membr-YFP). See Table 1 for statistical analysis of complete dataset.

not shown). However, the anti-Rin antibody only detected GFP–Rin and not GFP–Rit (data not shown), confirming its specificity. Thus, Rin protein appears to be expressed in neuronal, as well as non-neuronal, tissues and cell lines.

We next asked whether DAT and Rin interact in mammalian cells. Coimmunoprecipitations using an antibody directed against the DAT N terminus isolated Rin from DAT-PC12 cell lysates, confirming that Rin associates with DAT in mammalian neuroendocrine cells (Fig. 1*B*). Rin coimmunoprecipitated with DAT specifically and was not isolated from nontransfected PC12 cells, with antibodies directed against the transferrin receptor, or when empty Protein A/G beads were used (Fig. 1*B*). We also detected DAT/Rin interactions when DAT was immunoprecipitated from rat striatal synaptosomes (Fig. 1*C*), confirming that the DAT/Rin interaction occurs in brain. It should be noted that we were unable to detect the DAT/Rin interaction when a C-terminus-directed anti-DAT antibody was used for immunoprecipitation, despite quantitative DAT pull down (data not shown). Moreover, we were not able to perform the reciprocal coimmunoprecipitation, because the available Rin antibody does not effectively immunoprecipitate Rin.

Although the Rin monoclonal antibody recognizes a single band on immunoblots, it does not recognize Rin *in situ*, nor does it immunoisolate Rin from cell lysates. Furthermore, our attempts to raise rabbit anti-peptide antibodies against Rin domains divergent from its homolog Rit did not yield immunoreactive sera. Therefore, we used CFP-tagged Rin to ask whether DAT and Rin colocalize in cells and, if so, in what cellular regions. In PC12 cells cotransfected with CFP–Rin and DAT, staining was clearly detected as a ring around the cell perimeter (Fig. 2*A*), consistent with its predicted plasma membrane localization. CFP–Rin was also detected primarily at the cell perimeter (Fig. 2*A*), consistent with reports that it localizes to the plasma membrane (Heo et al., 2006). We observed substantial DAT and Rin colocalization at the plasma membrane, and DAT and Rin colocalization was limited to discrete foci within the plasma membrane (Fig. 2*A*, arrowheads). We also observed areas in which DAT did not appear to colocalize with Rin (Fig. 2*A*, arrows). DAT is distributed between lipid raft and non-raft microdomains within the plasma membrane (Adkins et al., 2007; Foster et al., 2008; Cremona et al., 2011), and we asked whether the focal distribution of DAT/Rin colocalization correlated with the expression of DAT in membrane microdomains. To answer this question, we coexpressed DAT and CFP–Rin and labeled lipid rafts with Alexa Fluor 594-conjugated CTX, which specifically labels membrane rafts via binding to GM1 ganglioside (Sandvig and van Deurs, 2000). Cells were then fixed, and DAT and CFP–Rin were stained as described in Materials and Methods, using Alexa Fluor 488- and Alexa Fluor 405-conjugated secondary antibodies to visualize DAT and Rin in the green and blue channels, respectively (Fig. 2*B*,*C*). Visually we observed striking colocalization of DAT and Rin in CTX-positive regions (Fig. 2*C*, arrowheads). We then quantitatively compared the percentage of DAT/Rin colocalization in CTX-positive versus CTX-negative regions. At virtually all the thresholds tested, there was more DAT/Rin colocalization in rafts than in non-rafts ($n = 16$). Only at a very few extreme thresholds for a few cells (data not shown) was DAT/Rin colocalization higher (by a small amount) in CTX-negative regions than in CTX-positive regions. Analysis at the median threshold values for each cell revealed significantly more DAT/Rin colocalization in raft versus non-raft populations (80.1 ± 2.4% in CTX-positive vs 57.0 ± 4.9% in CTX-negative regions; $p < 0.0001$, paired t test; $n = 16$).

Table 1. Statistical analysis of N_{FRET} values

FRET Pair #1	FRET Pair #2	Significant?
CFP–DAT + YFP–Rin	CFP–SERT + YFP–Rin	Yes*
CFP–DAT + YFP–Rin	CFP–rGAT1 + YFP–Rin	Yes*
CFP–DAT + YFP–Rin	CFP–TfR + YFP–TfR	NS
CFP–DAT + YFP–Rin	CFP–TfR + YFP–Rin	Yes*
CFP–DAT + YFP–Rin	CFP–Rin + YFP–Rin	Yes*
CFP–DAT + YFP–Rin	YFP–DAT + membr-CFP	Yes*
CFP–DAT + YFP–Rin	CFP–Rin + membr-YFP	Yes*
CFP–DAT + YFP–Rin	CFP–Rin + YFP–DAT	NS
CFP–DAT + YFP–Rin	CFP–DAT + YFP–DAT	NS
CFP–SERT + YFP–Rin	CFP–rGAT1 + YFP–Rin	NS
CFP–SERT + YFP–Rin	CFP–TfR + YFP–TfR	Yes*
CFP–SERT + YFP–Rin	CFP–TfR + YFP–Rin	NS
CFP–SERT + YFP–Rin	CFP–Rin + YFP–Rin	NS
CFP–SERT + YFP–Rin	YFP–DAT + membr-CFP	NS
CFP–SERT + YFP–Rin	CFP–Rin + membr-YFP	NS
CFP–SERT + YFP–Rin	CFP–Rin + YFP–DAT	Yes**
CFP–SERT + YFP–Rin	CFP–DAT + YFP–DAT	Yes*
CFP-rGAT1 + YFP–Rin	CFP–TfR + YFP–TfR	Yes*
CFP-rGAT1 + YFP–Rin	CFP–TfR + YFP–Rin	NS
CFP-rGAT1 + YFP–Rin	CFP–Rin + YFP–Rin	NS

*$p < 0.001$, **$p < 0.05$, one-way ANOVA with Dunn's multiple comparison test.

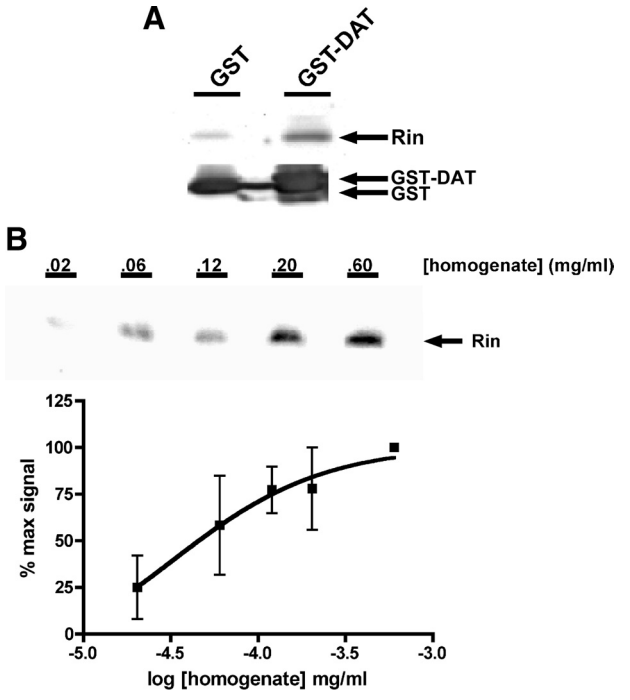


Figure 4. Rin interacts with the DAT C terminus. GST pull-down assays. PC12 homogenate was incubated with either GST or GST–DAT 587–617, 1 h, 37°C. Complexes were isolated with glutathione agarose, and Rin was detected by immunoblot as described in Materials and Methods. ***A***, Rin is isolated with the DAT C terminus but not GST alone. ***B***, Concentration dependence. GST–DAT 587–617 was incubated with increasing concentrations of PC12 homogenate, 1 h, 37°C, followed by isolation of complexes with glutathione agarose. Top, Representative immunoblot probed for Rin. Bottom, Averaged data. Results are expressed as percentage maximal Rin signal versus log PC12 homogenate concentration (milligrams per milliliters) and were fit to a sigmoidal dose–response curve ($r^2 = 0.98$, $n = 3$).

To further evaluate whether DAT and Rin directly interact in living cells, we used FRET microscopy (Schmid and Sitte, 2003) using the three-filter method (Xia and Liu, 2001) as described by Feige et al. (2005), which achieves quantitative visualization of protein oligomerization in intact cells and which generates N_{FRET} images. The results are shown in Figure 3 and Table 1. To provide

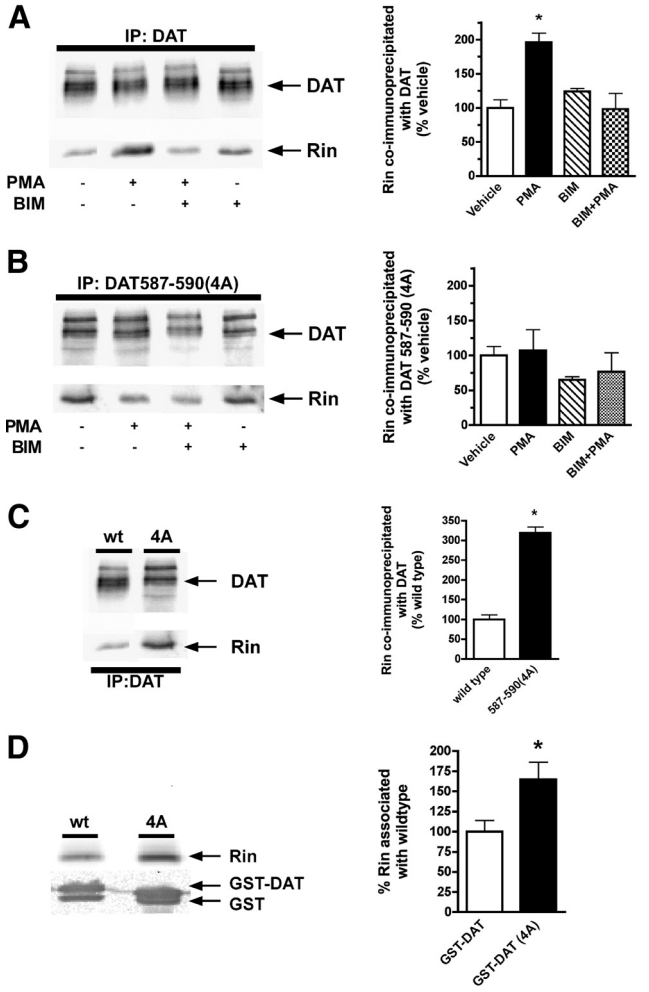


Figure 5. DAT/Rin interactions are regulated by PKC activation and are sensitive to DAT C-terminal residues 587–590. ***A–C***, Coimmunoprecipitations. PC12 cells stably expressing either wild-type DAT (***A***) or DAT 587–590(4A) (***B***) were pretreated with either 1 μM BIM or vehicle, 20 min, 37°C, followed by treatment with either vehicle or 1 μM PMA, 30 min, 37°C. Cells were lysed, and DAT was immunoprecipitated from equivalent amounts of cellular protein. Immunoprecipitants were resolved by SDS-PAGE and immunoblotted for both DAT and Rin. Left, Representative immunoblots. Right, Averaged data. Rin signals from nonsaturating bands were normalized to DAT signals and are expressed as percentage vehicle signal ± SEM. *$p <$ 0.002, significantly different from vehicle control (one-way ANOVA with Tukey's multiple comparison test; $n = 4$). ***C***, Basal Rin interaction with wild-type versus 587–590(4A) DAT. Left, Representative immunoblot. Right, Averaged data. Rin signals from nonsaturating bands were normalized to DAT signals and expressed as percentage wild-type signal ± SEM. *$p < 0.0005$, significantly different from wild-type DAT (Student's *t* test; $n = 3$). ***D***, GST pull downs. GST fused to either wild-type or DAT 587–590(4A) C termini were induced and isolated on glutathione sepharose as described in Materials and Methods. Equivalent amounts of GST–DAT fusion proteins were incubated with PC12 homogenates, and bound proteins were resolved by SDS-PAGE and immunoblotted for both Rin and GST. Left, Representative immunoblot. Right, Averaged data. Rin densities were normalized to total GST pulled down for each sample and are expressed as percentage ± SEM Rin isolated compared with wild-type GST–DAT. *$p < 0.04$, significantly different from wild-type GST–DAT (Student's *t* test; $n = 5$).

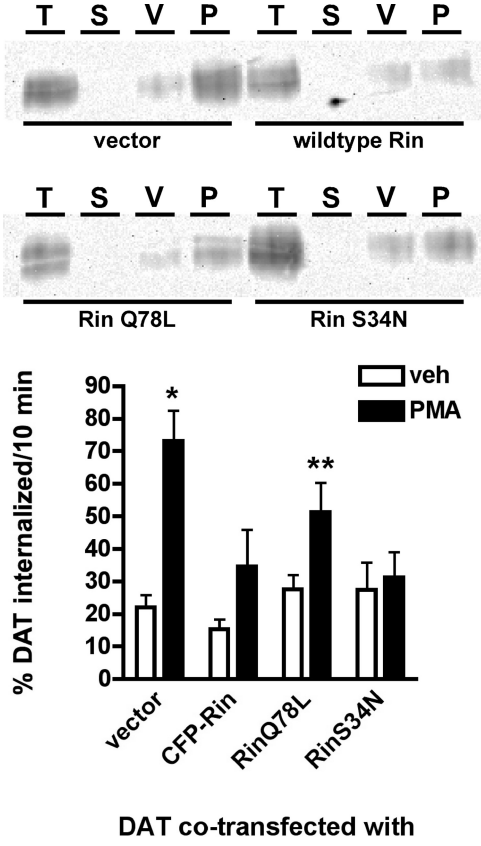


Figure 6. PKC-induced DAT internalization requires Rin activity. Internalization assays. PC12 cells were cotransfected with DAT and the indicated Rin or control cDNAs and were assayed 48–72 h after transfection. Relative DAT internalization rates over 10 min were measured by reversible biotinylation during treatment with or without 1 μM PMA, 37°C as described in Materials and Methods. Top, Representative immunoblots showing total surface DAT at time 0 (T), strip controls (S), and internalized DAT under vehicle-treated (V) and PMA-treated (P) conditions. Bottom, Average data. veh, Vehicle. Data are expressed as percentage ± SEM DAT internalized/10 min compared with total surface DAT at $t = 0$. *$p < 0.001$, **$p < 0.05$, significantly different from vehicle-treated control (Student's *t* test; $n = 4$).

a reference for membrane protein oligomerization, we coexpressed CFP- and YFP-tagged DAT, which have been shown to homo-oligomerize by both biochemical approaches (Hastrup et al., 2001; Sorkina et al., 2003; Miranda et al., 2004; Bartholomaus et al., 2008) and FRET microscopy in various cell lines (Sorkina et al., 2003; Miranda et al., 2004; Bartholomaus et al., 2008) and transfected neurons (Egaña et al., 2009). In addition, we used SERT tagged with CFP and YFP on its cytoplasmic N and C termini, respectively (C-SERT-Y), i.e., a transporter construct predicted to produce a strong homotypic FRET signal (Egaña et al., 2009). Coexpressing C-DAT and Y-DAT or C-SERT-Y resulted in enriched plasma membrane fluorescence and, as expected, robust N_{FRET} signals (18.89 ± 0. 1.16, $n = 23$ and 48.39 ± 2.54, $n = 28$, respectively; Fig. 3*B*, Table 1). Similarly, expressing fluorescently tagged Rin proteins resulted in predominant plasma membrane fluorescence (Fig. 3*A*). Coexpression of CFP–DAT and YFP–Rin resulted in an N_{FRET} value of 17.54 ± 1.30 ($n = 24$; Fig. 3*A*,*B*), which was significantly higher than fluorescent Rin proteins ($p < 0.001$, one-way ANOVA with Dunn's multiple comparison test) and not significantly different from either coexpressed CFP–DAT and YFP–DAT or CFP–Rin and YFP–DAT. This confirms that DAT and Rin interact in living cells and that the different fluorescent tags do not influence the signal. To control for the possibility of nonspecific FRET of fluorescent proteins in the plasma membrane, we tested whether Rin would generate significant FRET interaction with membrane anchored YFP; coexpression with CFP–Rin yielded an N_{FRET} value of 5.40 ± 0.49 ($n = 15$; Fig. 3*B*), which was significantly less than any DAT/Rin combination ($p < 0.001$). Apparently, this membrane-attached YFP can serve as a weak acceptor for CFP fluorophores attached to proteins integral to membranes; indeed, some spurious FRET signal was visible during coexpression with CFP–DAT, but only in a cytosolic compartment (data not

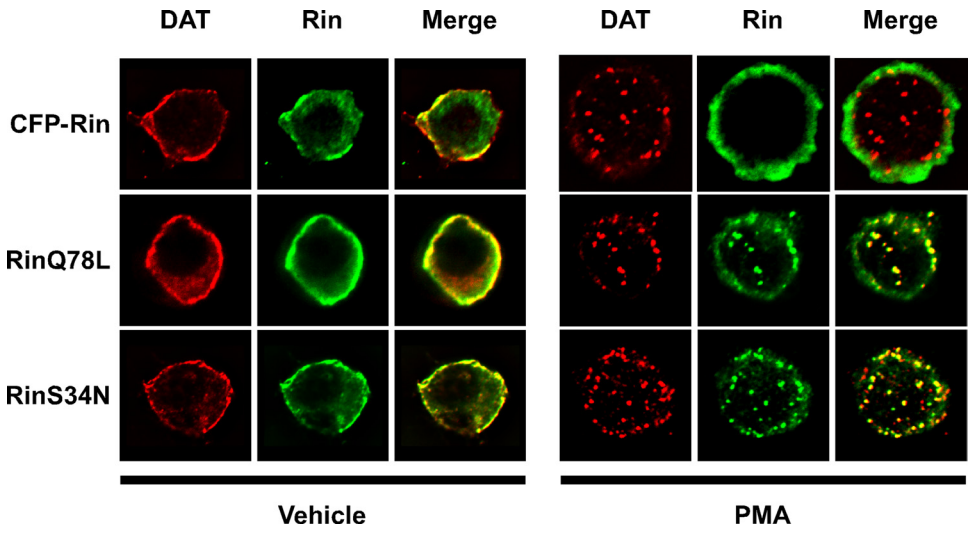


Figure 7. Guanyl nucleotide exchange is required for PKC-mediated Rin dissociation from DAT. Immunofluorescence. PC12 cells were cotransfected with DAT and the indicated Rin or control cDNAs and were assayed 48 h after transfection. Cells were treated with or without 1 μM PMA, 30 min, 37°C and were fixed, stained with anti-DAT or anti-GFP (to detect CFP–Rin) antibodies, and imaged as described in Materials and Methods. Planes through the cell center are shown and are representative of 12–16 cells imaged per condition in instances in which PMA-induced internalization was apparent ($n = 4$).

shown); therefore, the transitional interaction most likely occurred in the endoplasmic reticulum. Importantly, Rin proteins do not interact with themselves as revealed by an N_{FRET} value of 6.24 ± 0.90 ($n = 16$; Fig. 3*B*).

We next asked whether the interaction of Rin with DAT was specific to DAT or whether it extended either to other SLC6 transporters or generally to proteins that are rapidly endocytosis, such as the transferrin receptor (TfR). To test potential Rin interaction with other SLC6 neurotransmitter transporters, we coexpressed Rin with either fluorescently tagged rat GABA (CFP–GAT1) or human serotonin transporter (CFP–SERT). Interestingly, CFP–GAT1 and CFP–SERT did not interact with YFP–Rin (N_{FRET} values of 6.55 ± 0.64 and 7.58 ± 0.77, respectively; Fig. 3*A*,*B*). Neither condition differed significantly from the CFP–Rin and membrane YFP negative control, and rGAT1 and Rin were significantly less than from DAT and Rin ($p < 0.001$) and from the positive control CFP–TfR and YFP–TfR (N_{FRET} value of 18.53 ± 0.96) ($p < 0.001$) but not from hSERT and Rin (N_{FRET} value of 7.58 ± 0.77; $n = 27$), respectively (Fig. 3*B*). To test for Rin interactions with rapidly internalizing surface proteins, we coexpressed of YFP–Rin with CFP–TfR. This condition resulted in an N_{FRET} value of 6.35 ± 0.83, which was significantly less that DAT/Rin FRET pairs and not significantly greater than fluorescent Rin proteins or membrane-anchored fluorescent proteins with either DAT or Rin (Fig. 3*B*). Lack of a significant TfR/Rin FRET signal was not attributable to inability of fluorescently tagged TfR to form FRET pairs, because CFP–TfR and YFP–TfR coexpression resulted in an N_{FRET} value of 18.5 ± 0.96, which was significantly greater than fluorescent TfR with Rin and is consistent with the known TfR homodimerization (Fig. 3*B*) (Alvarez et al., 1989).

We next tested whether DAT/Rin interactions relied specifically on the DAT C terminus. To test this, we performed *in vitro* pull-down assays, using a GST fusion protein expressing DAT C-terminal residues 587–617 to probe PC12 cell homogenates lacking DAT expression. The GST–DAT 587–617 fusion protein was sufficient to isolate Rin from PC12 homogenates, whereas GST alone was not (Fig. 4*A*). Moreover, GST–DAT 587–617 recovered Rin from PC12 homogenates in a concentration-dependent manner (Fig. 4*B*). Together with our yeast two-hybrid co-IP and FRET data, these results demonstrate that DAT and Rin directly interact in mammalian cells and brain and that their interaction is mediated by the DAT C terminus, which encodes the FREKLAYAIA sequence used as bait in the original yeast two-hybrid screen.

PKC activation regulates DAT and Rin interactions

Our previous studies demonstrated that DAT residues 587–596 (FREKLAYAIA) encode elements that control DAT endocytic rates in a PKC-sensitive manner (Boudanova et al., 2008). Specifically, 587–589 (REK) residues are required for PKC-induced increases in DAT internalization. Moreover, mutating residues 587–590 accelerates basal DAT endocytic rates, suggesting that a negative regulatory mechanism controls DAT endocytic rates. Therefore, we asked whether DAT associations with Rin were regulated by PKC activation and whether residues in the 587–590 region played a role in DAT/Rin interactions. PC12 cells stably expressing either wild-type DAT or the DAT 587–590(4A) mutant were treated with 1 μM PMA, 30 min, 37°C, and DAT/Rin interactions were assessed by coimmunoprecipitation and immunoblot. PKC activation significantly increased wild-type DAT/Rin interactions to 183.6 ± 16.5% of basal DAT/Rin interactions ($p < 0.005$, Student's t test; $n = 4$) (Fig. 5*A*). PMA-induced increases in wild-type DAT/Rin interactions were blocked when cells were preincubated with the PKC inhibitor BIM (Fig. 5*A*), demonstrating that the PMA-induced increase in DAT/Rin interactions is PKC dependent. In contrast, PMA treatment did not significantly increase Rin interactions with DAT 587–590(4A) (Fig. 5*B*), and pretreatment with BIM did not alter DAT 587–590(4A)/Rin interactions. Moreover, under basal conditions, DAT 587–590(4A) interactions with Rin were 300% of wild-type DAT/Rin interactions (Fig. 5*C*). These results suggest that DAT residues 587–590 are required for PKC-induced increases in DAT/Rin interactions. Additionally, these results suggest that DAT/Rin interactions increase in conditions were DAT internalization rates are accelerated either by PKC activation or mutating residues 587–590. To further test this possibility, we performed GST pull downs using GST–DAT C terminus that

encoded the 587–590(4A) mutation [GST–DAT(4A)]. GST–DAT(4A) isolated significantly more Rin than wild-type GST–DAT (164.6 ± 21.8% of wild-type levels) (Fig. 5*D*), consistent with a role for residues 587–590 in modulating DAT/Rin interactions.

Rin is required for PKC-mediated DAT trafficking

We next asked whether DAT endocytosis requires Rin activity, under either basal or PKC-stimulated conditions. To address this question, we used reversible biotinylation to measure relative DAT internalization rates in PC12 cells coexpressing DAT with wild-type Rin, or constitutively active (Q78L) or dominant-negative (S34N) Rin mutants. The results are shown in Figure 6. DAT internalized robustly under control conditions and PMA treatment significantly increased the endocytic rate of DAT, both when DAT was coexpressed with empty vector or constitutively active RinQ78L. In contrast, coexpressing DAT with either wild-type Rin or dominant-negative Rin S34N completely inhibited PMA-stimulated DAT endocytosis but had no effect on basal DAT internalization rates. These results demonstrate that Rin activity is required for PKC stimulation of DAT endocytosis.

We also visually examined DAT surface levels in response to PKC activation when DAT was coexpressed with either wild-type or mutant Rin constructs. When DAT was coexpressed with either vector (data not shown) or CFP–Rin, we observed robust DAT and Rin surface expression under vehicle-treated conditions (Fig. 7). PMA treatment for 30 min, 37°C resulted in marked DAT redistribution to intracellular puncta, whereas Rin dissociated from DAT remained at the plasma membrane after PKC activation (Fig. 7). In cells that coexpressed DAT and Rin mutants, DAT and Rin were similarly expressed at the plasma membrane under vehicle conditions (Fig. 7). However, although both wild-type Rin and Rin S34N inhibited PKC-stimulated DAT internalization when the global population was examined by biochemical means (i.e., reversible biotinylation; Fig. 6), we still observed a subpopulation of cells that exhibit DAT intracellular sequestration in response to PKC activation. In this subpopulation, and in contrast to control conditions, both RinQ78L and S34N failed to dissociate from DAT and internalized with DAT into intracellular puncta after PKC activation (Fig. 7). The majority of intracellular Rin puncta colocalized with DAT, although some DAT puncta were without Rin colocalization. These results suggest that the ability of Rin to dissociate from DAT after PKC activation is dependent on its ability to exchange guanyl nucleotide.

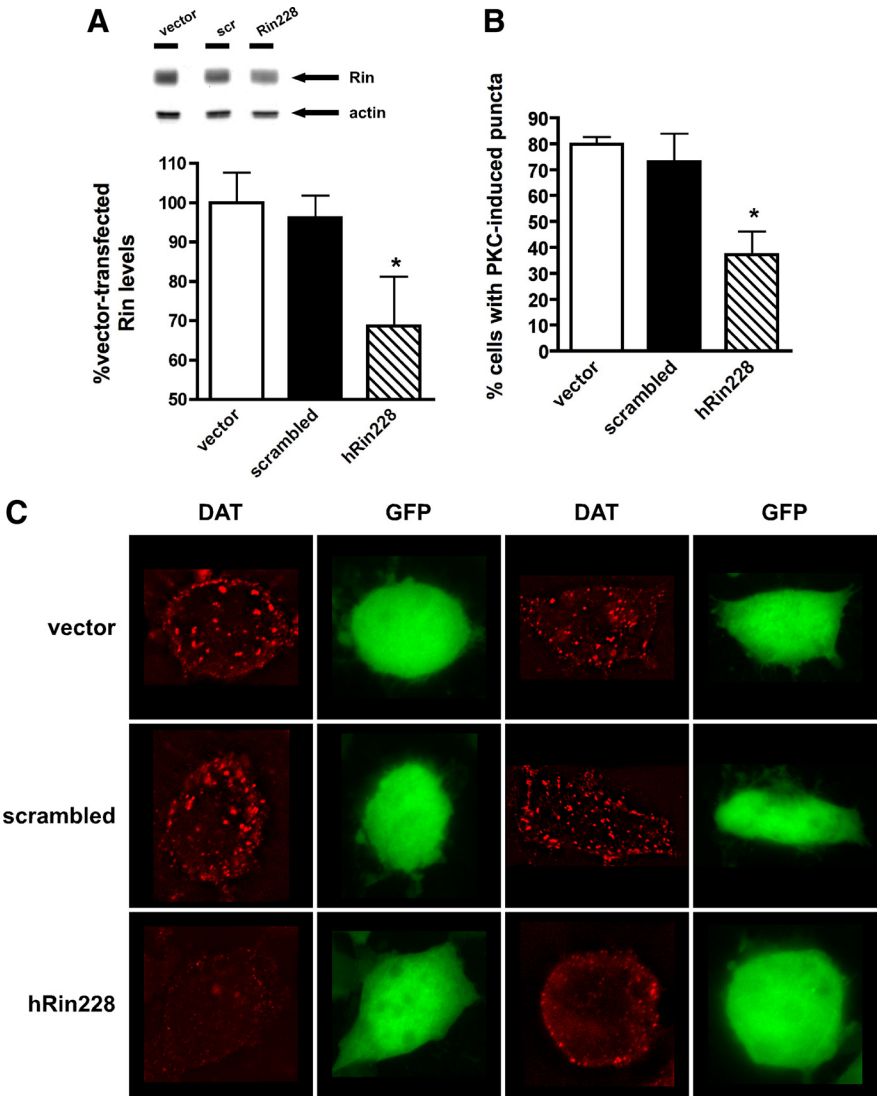


Figure 8. Rin is required for PKC-mediated DAT sequestration. hRin knockdown and antibody internalization assay. ***A***, hRin knockdown. hRin-directed shRNAs were screened in HEK293 cells, 72 h after transfection. Top, Representative immunoblot showing Rin levels in vector-transfected, scrambled shRNA-transfected (scr), and hRin228-transfected cells, with actin probed as a loading control. Bottom, Averaged data. Data are expressed as percentage Rin levels compared with vector-transfected cells (normalized to actin loading control). $*p < 0.05$, significantly different from vector control (one-way ANOVA with Dunnett's *post hoc* analysis; $n = 5$). ***B***, ***C***, Antibody internalization assay. SK-N-MC cells cotransfected with EL2–HA–DAT and the indicated constructs were assayed 72 h after transfection. Cells were labeled with HA antibody, and DAT internalization was assessed for 15 min, 37°C in the presence of 1 μM PMA as described in Materials and Methods. Cells expressing shRNA constructs were identified by GFP coexpression. Optical *z*-stacks were collected and deconvolved as described in Materials and Methods. ***B***, Averaged data. Data are expressed as percentage ± SEM cells exhibiting PMA-induced intracellular DAT puncta for each of the indicated transfection conditions. $*p < 0.05$, significantly different from vector-transfected control (one-way ANOVA with Dunnett's multiple comparison test; $n = 3$). ***C***, Representative images. Planes through the cell center are shown for two cells per condition and are representative of 30–34 cells imaged per condition over three independent experiments.

We further tested whether Rin was required for PKC-mediated DAT trafficking, using shRNAs targeted against human Rin mRNA to knockdown cellular Rin levels. Three shRNAs were tested for their ability to reduce cellular Rin levels in HEK293 cells. Of these, hRin228 significantly reduced Rin levels down to 68.6 ± 12.6% of that observed in vector-transfected cells, whereas a scrambled shRNA had no effect on Rin levels (Fig. 8*B*, inset). Using these Rin-directed shRNAs, we first asked whether Rin was required for PKC-induced DAT sequestration in the human neuroblastoma cell line SK-N-MC. This line was chosen because it expresses the dopamine biosynthetic enzyme tyrosine

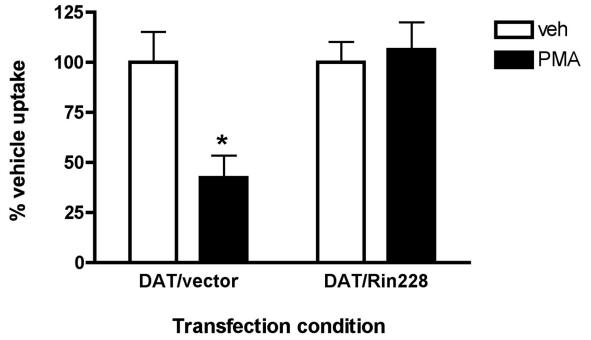


Figure 9. Rin is required for PKC-induced DAT functional downregulation. [^{3}H]DA uptake assays. SK-N-MC cells were cotransfected with DAT and the indicated constructs, and [^{3}H]DA uptake was assessed 72 h after transfection. Cells were treated with or without 1 μM PMA, 30 min, 37°C, followed by addition of [^{3}H]DA as described in Materials and Methods. Averaged data are shown and are expressed as percentage ± SEM uptake of vehicle-treated cells. *$p <$ 0.03, significantly different from vehicle-treated control (Student's *t* test; $n = 4$).

hydroxylase (Z.H.S., M.J.K., and H.E.M., unpublished data) and is compatible with commercially available human-targeted shRNAs. We coexpressed DAT encoding an extracellular HA epitope tag in the second extracellular loop with control or Rin-directed shRNA vectors and assessed PMA-induced DAT endocytosis by labeling surface DAT with anti-HA antibody. In cells cotransfected with DAT and GFP-expressing vector, treatment with 1 μM PMA treatment, 15 min, 37°C resulted in robust DAT intracellular puncta in 79.8 ± 2.9% of cells (Fig. 8). Coexpressing DAT with scrambled shRNA had no significant effect on the number of cells exhibiting PMA-induced DAT internalization (73.0 ± 11.0% of cells). In contrast, significantly fewer cells exhibited PMA-induced DAT internalization when coexpressed with hRin228 (37.2 ± 8.9% cells; $p < 0.05$, one-way ANOVA with Dunnett's *post hoc* analysis). Rin knockdown effects on DAT internalization were not attributable to global perturbation of the endocytic machinery, because TfR endocytosis was identical in vector- versus hRin228-transfected cells, as assessed by Alexa Fluor 594–transferrin uptake (data not shown). These results demonstrate that Rin is absolutely essential for PKC-induced DAT sequestration.

Given that Rin is required for PKC-induced DAT sequestration, we used the hRin228 shRNA to ask whether Rin was required for PKC-mediated DAT functional downregulation. We measured robust [^{3}H]DA uptake in cells cotransfected with DAT and vector, and PKC activation significantly decreased DA uptake to 42.6 ± 11.1% of vehicle-treated cells ($p < 0.03$, Student's *t* test; $n = 4$; Fig. 9). In contrast, PKC activation had no significant effect on DA uptake in cells cotransfected with DAT and hRin228 (106.3 ± 13.7% of vehicle-treated cells; $p = 0.72$, Student's *t* test; $n = 4$; Fig. 9), consistent with the inability of DAT to sequester in a Rin-depleted environment.

Discussion

In the current study, we sought to identify proteins that interacted with DAT residues 587–596 and were central to PKC-induced DAT sequestration. Using the hSOS rescue yeast two-hybrid approach, we determined that the neuronal GTPase Rin (Rit2) interacts with DAT residues 587–596 (FREKLAYAIA) and that Rin is absolutely required for PKC-induced DAT sequestration. Rin, also known as Rit2, is a member of the Rit subfamily of Ras-like small GTPases, which also includes the *Drosophila* homolog RIC (Wes et al., 1996). These GTPases are highly conserved and are distinguished from other Ras-like GTPases in their lack of a C-terminal CaaX box for prenylation. Recent evidence suggests that a polybasic charged domain conserved at their C termini facilitates their plasma membrane association (Heo et al., 2006). Whereas Rit is ubiquitously expressed, Rin expression is reported to be limited to neurons (Lee et al., 1996), and a recent report suggests that Rin expression is particularly enriched in dopaminergic neurons (Zhou et al., 2011). A recent study also revealed that Rin exhibits significant copy number variation in schizophrenic patient populations (Glessner et al., 2010) and that a 5.3 Mb deletion encompassing the Rin gene on chromosome 18q12.3 is present in two patients with profound speech delay (Bouquillon et al., 2011). Together, these results suggest that Rin may play a central role in the pathophysiology of neuropsychiatric disorders.

What is known about the role of Rin in intracellular signaling, and how might that shed light onto downstream pathways that converge on DAT? Rin activates atypical PKC via interactions with the Par6/cdc42 complex (Hoshino and Nakamura, 2003; Hoshino et al., 2005) and a recent screen for endocytic determinants in *Caenorhabditis elegans* revealed that the Par6/cdc42 complex is absolutely required for transferrin receptor endocytosis, as well as for MHCI endocytic recycling (Balklava et al., 2007). Additionally, the Par6/cdc42/aPKC complex is required for E-cadherin endocytosis in *Drosophila* (Leibfried et al., 2008). Our results linking Rin to regulated DAT internalization raise the possibility that Rin may be an upstream signaling step in Par6/cdc42-dependent endocytosis. Rin also reportedly binds to and activates calmodulin (Lee et al., 1996). Given that CaMKII interacts with the DAT C terminus and is essential for amphetamine-mediated DA efflux through DAT (Fog et al., 2006), it is possible that Rin may serve as a means to activate DAT-bound CaMKII via calmodulin activation. Rin is also required for nerve growth factor (NGF)-stimulated neurite extension (Spencer et al., 2002a,b; Lein et al., 2007) and p38 MAP kinase activation in response to NGF signaling (Shi et al., 2005). Several reports link the MAP kinase signaling pathway to DAT trafficking (Morón et al., 2003; Bolan et al., 2007; Zapata et al., 2007; Mortensen et al., 2008), potentially implicating Rin in this process as well.

We detected Rin protein expression in striatal tissue and several dopaminergic cell lines, including SK-N-MC and PC12 (Fig. 1*A*). In addition, we detected Rin in non-neuronal tissues and cell lines (data not shown), whereas previous studies reported that Rin mRNA expression was limited to neuronal tissues as determined by Northern blot and RT-PCR approaches (Lee et al., 1996). This inconsistency is not attributable to lack of specificity of the Rin antibody, because it did not cross-react with GFP–Rit (data not shown). Moreover, we detected both Rit and Rin mRNA signals by RT-PCR in primary mouse embryonic kidney, PC12, and HeLa cells, as well as in whole brain and substantia nigra (data not shown). Thus, the apparent discrepancy between our results and previous reports may reflect a lack in sensitivity in the available approaches used at the time the previous studies were performed. Alternatively, Rin may be ectopically expressed in transformed cell lines.

We observed DAT/Rin associations via coimmunoprecipitation in rat striatal tissue (Fig. 1) and PC12 cells (Figs. 1, 5). Additionally, colocalization studies revealed that the DAT/Rin interaction occurs at the plasma membrane in PC12 and HEK293 cell lines (Figs. 2, 3, 6). We also wanted to determine whether DAT and Rin colocalize in native dopaminergic neurons. The commercially available Rin monoclonal antibody does not recognize Rin *in situ*, and our attempts at raising Rin-specific antisera were not successful, thwarting our ability to examine the DAT/Rin interaction in native preparations. As an alternative, we

attempted to express CFP–Rin in primary ventral midbrain (VM) neurons using lentiviral infection. Despite successful generation of high-titer lentivirus, as determine by transduction of HEK293 cells, we were unable to reproducibly and efficiently transduce VM neurons in culture. Future studies will explore alternative gene delivery methods to further examine the DAT/Rin interaction *in situ*.

DAT/Rin interactions were significantly enriched in membrane raft regions within the membrane (Fig. 2*B–D*). A recent report indicates that DAT localizes to both lipid raft and non-raft domains within the plasma membrane (Foster et al., 2008) and that DAT may be differentially regulated by PKC, depending on its microdomain localization. Moreover, Cremona et al. (2011) recently reported that the membrane raft protein flotilin-1 is absolutely required for DAT localization to lipid microdomains and for PKC-stimulated DAT sequestration. Thus, DAT/Rin interactions may occur in a specific lipid microdomain that facilitates enhanced endocytosis in response to PKC activation.

We recently reported that the charged residues at hDAT positions E589 and R590 contribute to a braking mechanism that dampens DAT endocytic rates under basal conditions but is released during PKC activation (Boudanova et al., 2008). In agreement with our findings, Sorkina et al. (2009) also recently confirmed the existence of a negative endocytic regulatory mechanism. Interestingly, results from that study demonstrated that the negative endocytic regulatory mechanism requires the DAT N terminus. The DAT N terminus is also the target of PKC-stimulated ubiquitination, and ubiquitination is required for PKC-mediated DAT internalization (Miranda et al., 2007). We observed increased DAT/Rin interactions in circumstances in which the DAT endocytic brake is released, either during PKC activation (Fig. 5*A*) or when DAT residues 587–590 are mutated (Fig. 5*C*,*D*). These results suggest that Rin plays a role in accelerating DAT endocytic rates. It also raises the possibility that there is a synergistic interaction between the DAT N and C termini that regulates the DAT endocytic rate.

A common approach to testing the role of small GTPases is the use of dominant-negative and constitutively active mutant GTPases, which are locked in the GTP-bound and GDP-bound states, respectively, and are unable to either hydrolyze GTP (constitutively active) or exchange GDP for GTP (dominant negative). Rin Q78L and S34N mutants have been described previously to perturb Rin function in response to growth factor stimulation (Shi et al., 2005; Andres et al., 2006). The Rin S34N mutant inhibited PKC-mediated DAT sequestration (Fig. 6), consistent with a requisite role for Rin in PKC regulated DAT endocytosis. Interestingly, overexpression of wild-type Rin also inhibited PKC-stimulated DAT endocytosis. Overexpressed GTPases can have an inhibitory effect, because they can mislocalize and potentially sequester important factors required for vesicle trafficking (Shipitsin and Feig, 2004). Cellular imaging revealed that both of the Rin mutants fail to dissociate from DAT during internalization (Fig. 7). Together with our coimmunoprecipitation results, these data suggest that Rin binds to the DAT C terminus to promote increased DAT internalization rates and then dissociates from DAT during guanyl nucleotide exchange. Rab GTPases are reported to function in a similar manner, with guanyl nucleotide exchange dictating Rab movement between membrane-bound compartments (Goody et al., 2005).

Rin depletion significantly inhibited PKC-mediated DAT sequestration (Fig. 8). However, we should note that we did see PKC-induced DAT internalization in a population of cells with either high DAT expression or relatively low shRNA expression (correlated to GFP signal intensity). This is consistent with our previous report in which we observed that PKC-mediated DAT trafficking is highly sensitive to DAT expression levels (Loder and Melikian, 2003), suggesting a readily saturable cellular process. Indeed, we also observed that excessively high DAT expression levels in HEK293 cells resulted in a loss of PKC-induced DAT sequestration (Z.H.S. and H.E.M., unpublished results). Surprisingly, Rin knockdown also abolished PKC-mediated DAT functional downregulation (Fig. 9). Foster et al. (2008) recently reported both trafficking-dependent and -independent modes of PKC-mediated DAT downregulation, in contrast with our findings. The differences in our results may be attributable to different cell lines used (LLC-PK1 vs SK-N-MC) or may indicate that Rin is also required for trafficking-independent forms of PKC-mediated DAT downregulation. One possibility is that distinct PKC isoforms may participate in trafficking-dependent and -independent DAT regulatory mechanisms. A recent report suggests that PKCβ plays a central role in DAT trafficking (Chen et al., 2009). In addition, previous studies demonstrated that multiple PKC isoforms are capable of functional DAT downregulation (Doolen and Zahniser, 2002). Because phorbol ester treatment activates multiple PKC isoforms, simultaneously, we cannot conclude whether or not specific PKC isoforms underlie the trafficking-dependent and -independent forms of DAT downregulation. However, future studies exploring the role of specific PKC isoforms in Rin-mediated DAT trafficking should be illuminating in this regard.

Recent studies have revealed a central role for biogenic amine transporter function in neuropsychiatric disorders, including ADHD (Mazei-Robison et al., 2008) and autism (Prasad et al., 2009). Given the eminent role that transporters play, both as addictive and therapeutic drug targets, as well as in the pathophysiology of neuropsychiatric diseases, modulation of transporter availability by membrane trafficking is likely to have a significant impact on both normal and aberrant neurotransmission. The identification of Rin as a critical modulator of DAT trafficking and as a potentially important link between DAT, CaMKII, and MAP kinase signaling will undoubtedly shed additional light on the mechanisms governing dopamine levels and plasticity in the brain. Moreover, these studies raise the possibility that Rin may play a larger role in synaptic endocytic trafficking.

References

Adkins EM, Samuvel DJ, Fog JU, Eriksen J, Jayanthi LD, Vaegter CB, Ramamoorthy S, Gether U (2007) Membrane mobility and microdomain association of the dopamine transporter studied with fluorescence correlation spectroscopy and fluorescence recovery after photobleaching. Biochemistry 46:10484–10497.

Alvarez E, Gironès N, Davis RJ (1989) Intermolecular disulfide bonds are not required for the expression of the dimeric state and functional activity of the transferrin receptor. EMBO J 8:2231–2240.

Andres DA, Rudolph JL, Sengoku T, Shi GX (2006) Analysis of Rit signaling and biological activity. Methods Enzymol 407:499–512.

Balklava Z, Pant S, Fares H, Grant BD (2007) Genome-wide analysis identifies a general requirement for polarity proteins in endocytic traffic. Nat Cell Biol 9:1066–1073.

Bartholomäus I, Milan-Lobo L, Nicke A, Dutertre S, Hastrup H, Jha A, Gether U, Sitte HH, Betz H, Eulenburg V (2008) Glycine transporter dimers: evidence for occurrence in the plasma membrane. J Biol Chem 283:10978–10991.

Bjerggaard C, Fog JU, Hastrup H, Madsen K, Loland CJ, Javitch JA, Gether U (2004) Surface targeting of the dopamine transporter involves discrete epitopes in the distal C terminus but does not require canonical PDZ domain interactions. J Neurosci 24:7024–7036.

Bolan EA, Kivell B, Jaligam V, Oz M, Jayanthi LD, Han Y, Sen N, Urizar E, Gomes I, Devi LA, Ramamoorthy S, Javitch JA, Zapata A, Shippenberg TS

(2007) D2 receptors regulate dopamine transporter function via an extracellular signal-regulated kinases 1 and 2-dependent and phosphoinositide 3 kinase-independent mechanism. Mol Pharmacol 71:1222–1232.

Boudanova E, Navaroli DM, Stevens Z, Melikian HE (2008) Dopamine transporter endocytic determinants: carboxy terminal residues critical for basal and PKC-stimulated internalization. Mol Cell Neurosci 39:211–217.

Bouquillon S, Andrieux J, Landais E, Duban-Bedu B, Boidein F, Lenne B, Vallée L, Leal T, Doco-Fenzy M, Delobel B (2011) A 5.3Mb deletion in chromosome 18q12.3 as the smallest region of overlap in two patients with expressive speech delay. Eur J Med Genet 54:194–197.

Carneiro AM, Ingram SL, Beaulieu JM, Sweeney A, Amara SG, Thomas SM, Caron MG, Torres GE (2002) The multiple LIM domain-containing adaptor protein Hic-5 synaptically colocalizes and interacts with the dopamine transporter. J Neurosci 22:7045–7054.

Chen R, Tilley MR, Wei H, Zhou F, Zhou FM, Ching S, Quan N, Stephens RL, Hill ER, Nottoli T, Han DD, Gu HH (2006) Abolished cocaine reward in mice with a cocaine-insensitive dopamine transporter. Proc Natl Acad Sci USA 103:9333–9338.

Chen R, Furman CA, Zhang M, Kim MN, Gereau RW 4th, Leitges M, Gnegy ME (2009) Protein kinase Cbeta is a critical regulator of dopamine transporter trafficking and regulates the behavioral response to amphetamine in mice. J Pharmacol Exp Ther 328:912–920.

Cremona ML, Matthies HJ, Pau K, Bowton E, Speed N, Lute BJ, Anderson M, Sen N, Robertson SD, Vaughan RA, Rothman JE, Galli A, Javitch JA, Yamamoto A (2011) Flotillin-1 is essential for PKC-triggered endocytosis and membrane microdomain localization of DAT. Nat Neurosci 14:469–477.

Doolen S, Zahniser NR (2002) Conventional protein kinase C isoforms regulate human dopamine transporter activity in *Xenopus* oocytes. FEBS Lett 516:187–190.

Egaña LA, Cuevas RA, Baust TB, Parra LA, Leak RK, Hochendoner S, Peña K, Quiroz M, Hong WC, Dorostkar MM, Janz R, Sitte HH, Torres GE (2009) Physical and functional interaction between the dopamine transporter and the synaptic vesicle protein synaptogyrin-3. J Neurosci 29:4592–4604.

Feige JN, Sage D, Wahli W, Desvergne B, Gelman L (2005) PixFRET, an ImageJ plug-in for FRET calculation that can accommodate variations in spectral bleed-throughs. Microsc Res Tech 68:51–58.

Fog JU, Khoshbouei H, Holy M, Owens WA, Vaegter CB, Sen N, Nikandrova Y, Bowton E, McMahon DG, Colbran RJ, Daws LC, Sitte HH, Javitch JA, Galli A, Gether U (2006) Calmodulin kinase II interacts with the dopamine transporter C terminus to regulate amphetamine-induced reverse transport. Neuron 51:417–429.

Foster JD, Adkins SD, Lever JR, Vaughan RA (2008) Phorbol ester induced trafficking-independent regulation and enhanced phosphorylation of the dopamine transporter associated with membrane rafts and cholesterol. J Neurochem 105:1683–1699.

Gainetdinov RR, Jones SR, Fumagalli F, Wightman RM, Caron MG (1998) Re-evaluation of the role of the dopamine transporter in dopamine system homeostasis. Brain Res Brain Res Rev 26:148–153.

Glessner JT, Reilly MP, Kim CE, Takahashi N, Albano A, Hou C, Bradfield JP, Zhang H, Sleiman PM, Flory JH, Imielinski M, Frackelton EC, Chiavacci R, Thomas KA, Garris M, Otieno FG, Davidson M, Weiser M, Reichenberg A, Davis KL, et al. (2010) Strong synaptic transmission impact by copy number variations in schizophrenia. Proc Natl Acad Sci USA 107:10584–10589.

Goody RS, Rak A, Alexandrov K (2005) The structural and mechanistic basis for recycling of Rab proteins between membrane compartments. Cell Mol Life Sci 62:1657–1670.

Hastrup H, Karlin A, Javitch JA (2001) Symmetrical dimer of the human dopamine transporter revealed by cross-linking Cys-306 at the extracellular end of the sixth transmembrane segment. Proc Natl Acad Sci USA 98:10055–10060.

Hein P, Frank M, Hoffmann C, Lohse MJ, Bünemann M (2005) Dynamics of receptor/G protein coupling in living cells. EMBO J 24:4106–4114.

Heo WD, Inoue T, Park WS, Kim ML, Park BO, Wandless TJ, Meyer T (2006) PI(3,4,5)P3 and PI(4,5)P2 lipids target proteins with polybasic clusters to the plasma membrane. Science 314:1458–1461.

Holton KL, Loder MK, Melikian HE (2005) Nonclassical, distinct endocytic signals dictate constitutive and PKC-regulated neurotransmitter transporter internalization. Nat Neurosci 8:881–888.

Hoshino M, Nakamura S (2003) Small GTPase Rin induces neurite outgrowth through Rac/Cdc42 and calmodulin in PC12 cells. J Cell Biol 163:1067–1076.

Hoshino M, Yoshimori T, Nakamura S (2005) Small GTPase proteins Rin and Rit Bind to PAR6 GTP-dependently and regulate cell transformation. J Biol Chem 280:22868–22874.

Iversen L (2006) Neurotransmitter transporters and their impact on the development of psychopharmacology. Br J Pharmacol 147:S82–S88.

Jones SR, Gainetdinov RR, Jaber M, Giros B, Wightman RM, Caron MG (1998) Profound neuronal plasticity in response to inactivation of the dopamine transporter. Proc Natl Acad Sci USA 95:4029–4034.

Just H, Sitte HH, Schmid JA, Freissmuth M, Kudlacek O (2004) Identification of an additional interaction domain in transmembrane domains 11 and 12 that supports oligomer formation in the human serotonin transporter. J Biol Chem 279:6650–6657.

Lee CH, Della NG, Chew CE, Zack DJ (1996) Rin, a neuron-specific and calmodulin-binding small G-protein, and Rit define a novel subfamily of ras proteins. J Neurosci 16:6784–6794.

Leibfried A, Fricke R, Morgan MJ, Bogdan S, Bellaiche Y (2008) *Drosophila* Cip4 and WASp define a branch of the Cdc42-Par6-aPKC pathway regulating E-cadherin endocytosis. Curr Biol 18:1639–1648.

Lein PJ, Guo X, Shi GX, Moholt-Siebert M, Bruun D, Andres DA (2007) The novel GTPase Rit differentially regulates axonal and dendritic growth. J Neurosci 27:4725–4736.

Loder MK, Melikian HE (2003) The dopamine transporter constitutively internalizes and recycles in a protein kinase C-regulated manner in stably transfected PC12 cell lines. J Biol Chem 278:22168–22174.

Mazei-Robison MS, Bowton E, Holy M, Schmudermaier M, Freissmuth M, Sitte HH, Galli A, Blakely RD (2008) Anomalous dopamine release associated with a human dopamine transporter coding variant. J Neurosci 28:7040–7046.

Melikian HE (2004) Neurotransmitter transporter trafficking: endocytosis, recycling, and regulation. Pharmacol Ther 104:17–27.

Melikian HE, Buckley KM (1999) Membrane trafficking regulates the activity of the human dopamine transporter. J Neurosci 19:7699–7710.

Miranda M, Sorkina T, Grammatopoulos TN, Zawada WM, Sorkin A (2004) Multiple molecular determinants in the carboxyl terminus regulate dopamine transporter export from endoplasmic reticulum. J Biol Chem 279:30760–30770.

Miranda M, Dionne KR, Sorkina T, Sorkin A (2007) Three ubiquitin conjugation sites in the amino terminus of the dopamine transporter mediate protein kinase C-dependent endocytosis of the transporter. Mol Biol Cell 18:313–323.

Morón JA, Zakharova I, Ferrer JV, Merrill GA, Hope B, Lafer EM, Lin ZC, Wang JB, Javitch JA, Galli A, Shippenberg TS (2003) Mitogen-activated protein kinase regulates dopamine transporter surface expression and dopamine transport capacity. J Neurosci 23:8480–8488.

Mortensen OV, Larsen MB, Prasad BM, Amara SG (2008) Genetic complementation screen identifies a mitogen-activated protein kinase phosphatase, MKP3, as a regulator of dopamine transporter trafficking. Mol Biol Cell 19:2818–2829.

Prasad HC, Steiner JA, Sutcliffe JS, Blakely RD (2009) Enhanced activity of human serotonin transporter variants associated with autism. Philos Trans R Soc Lond B Biol Sci 364:163–173.

Sandvig K, van Deurs B (2000) Entry of ricin and Shiga toxin into cells: molecular mechanisms and medical perspectives. EMBO J 19:5943–5950.

Schmid JA, Sitte HH (2003) Fluorescence resonance energy transfer in the study of cancer pathways. Curr Opin Oncol 15:55–64.

Shi GX, Han J, Andres DA (2005) Rin GTPase couples nerve growth factor signaling to p38 and b-Raf/ERK pathways to promote neuronal differentiation. J Biol Chem 280:37599–37609.

Shipitsin M, Feig LA (2004) RalA but not RalB enhances polarized delivery of membrane proteins to the basolateral surface of epithelial cells. Mol Cell Biol 24:5746–5756.

Sorkina T, Doolen S, Galperin E, Zahniser NR, Sorkin A (2003) Oligomerization of dopamine transporters visualized in living cells by fluorescence resonance energy transfer microscopy. J Biol Chem 278:28274–28283.

Sorkina T, Miranda M, Dionne KR, Hoover BR, Zahniser NR, Sorkin A (2006) RNA interference screen reveals an essential role of Nedd4–2 in dopamine transporter ubiquitination and endocytosis. J Neurosci 26:8195–8205.

Sorkina T, Richards TL, Rao A, Zahniser NR, Sorkin A (2009) Negative

regulation of dopamine transporter endocytosis by membrane-proximal N-terminal residues. J Neurosci 29:1361–1374.

Spencer ML, Shao H, Tucker HM, Andres DA (2002a) Nerve growth factor-dependent activation of the small GTPase Rin. J Biol Chem 277:17605–17615.

Spencer ML, Shao H, Andres DA (2002b) Induction of neurite extension and survival in pheochromocytoma cells by the Rit GTPase. J Biol Chem 277:20160–20168.

Sucic S, Dallinger S, Zdrazil B, Weissensteiner R, Jørgensen TN, Holy M, Kudlacek O, Seidel S, Cha JH, Gether U, Newman AH, Ecker GF, Freissmuth M, Sitte HH (2010) The N terminus of monoamine transporters is a lever required for the action of amphetamines. J Biol Chem 285:10924–10938.

Torres GE, Amara SG (2007) Glutamate and monoamine transporters: new visions of form and function. Curr Opin Neurobiol 17:304–312.

Torres GE, Yao WD, Mohn AR, Quan H, Kim KM, Levey AI, Staudinger J, Caron MG (2001) Functional interaction between monoamine plasma membrane transporters and the synaptic PDZ domain-containing protein PICK1. Neuron 30:121–134.

Torres GE, Gainetdinov RR, Caron MG (2003) Plasma membrane monoamine transporters: structure, regulation and function. Nat Rev Neurosci 4:13–25.

Wes PD, Yu M, Montell C (1996) RIC, a calmodulin-binding Ras-like GTPase. EMBO J 15:5839–5848.

Xia Z, Liu Y (2001) Reliable and global measurement of fluorescence resonance energy transfer using fluorescence microscopes. Biophys J 81:2395–2402.

Zapata A, Kivell B, Han Y, Javitch JA, Bolan EA, Kuraguntla D, Jaligam V, Oz M, Jayanthi LD, Samuvel DJ, Ramamoorthy S, Shippenberg TS (2007) Regulation of dopamine transporter function and cell surface expression by D3 dopamine receptors. J Biol Chem 282:35842–35854.

Zhou Q, Li J, Wang H, Yin Y, Zhou J (2011) Identification of nigral dopaminergic neuron-enriched genes in adult rats. Neurobiol Aging 32:313–326.